

GPSense: Passive Sensing with Pervasive GPS Signals

Huixin Dong^{†*}, Minhao Cui^{‡*}, Ning Wang[†], Lili Qiu[◊], Jie Xiong^{◊‡}, Wei Wang^{†★}

[†]Huazhong University of Science and Technology

[◊]Microsoft Research Asia, [‡]University of Massachusetts Amherst

{huixin,ningw,weiwangw}@hust.edu.cn, {minhaocui,jxiong}@cs.umass.edu, liliqiu@microsoft.com

ABSTRACT

Wireless sensing is gaining increasing attention from both academia and industry. Various wireless signals, such as Wi-Fi, UWB, and acoustic signals, have been leveraged for sensing. While promising in many aspects, two critical limitations still exist: a) limited sensing coverage; and b) the requirement for dedicated sensing signals, which may interfere with the original function of the wireless technology. To address these issues, we propose to utilize GPS signals for sensing, as GPS signals are already pervasive and emitted from satellites 24/7 at pre-allocated frequency bands, causing no interference. To make GPS sensing possible, we reconstruct signals with amplitude and phase information which is critical for sensing using the raw measurements reported by commercial GPS receiver module. We also develop sensing models to tailor the unique properties of GPS signals such as extremely long transmission distance. Finally, we introduce the concept of distributed sensing and design signal processing methods to fuse signals from multiple satellites to improve sensing performance. With all these designs, we prototype the first GPS wireless sensing system on commercial GPS receiver modules. Comprehensive experiments demonstrate that the proposed system can realize meaningful sensing applications such as human activity sensing, passive trajectory tracking, and respiration monitoring.

CCS CONCEPTS

- Human-centered computing → Ubiquitous and mobile computing systems and tools.

*Co-primary authors.

★Corresponding author.

Permission to make digital or hard copies of part or all of this work for personal or classroom use is granted without fee provided that copies are not made or distributed for profit or commercial advantage and that copies bear this notice and the full citation on the first page. Copyrights for third-party components of this work must be honored. For all other uses, contact the owner/author(s).

ACM MobiCom '24, November 18-22, 2024, Washington D.C., DC, USA

© 2024 Copyright held by the owner/author(s).

ACM ISBN 979-8-4007-0489-5/24/09.

<https://doi.org/10.1145/3636534.3690674>

KEYWORDS

GPS sensing; Pervasive sensing; Wireless sensing

ACM Reference Format:

Huixin Dong^{†*}, Minhao Cui^{‡*}, Ning Wang[†], Lili Qiu[◊], Jie Xiong^{◊‡}, Wei Wang^{†★}. 2024. GPSense: Passive Sensing with Pervasive GPS Signals. In *International Conference On Mobile Computing And Networking (ACM MobiCom '24), November 18-22, 2024, Washington D.C., DC, USA*. ACM, New York, NY, USA, 15 pages. <https://doi.org/10.1145/3636534.3690674>

1 INTRODUCTION

Since Marconi's first wireless transmission in 1894, wireless technologies have progressively become an indispensable part of our everyday life. In addition to their primary communication function, exemplified by the prevalent Wi-Fi and 4G services [7], wireless signals traditionally used for communication (e.g., Wi-Fi) have recently been exploited for sensing purposes [27, 47, 49, 56]. The basic principle behind passive wireless sensing is that signal propagation gets affected by human motions, which can be inferred by analyzing the induced signal variations. The human motions range from relatively large motions such as hand gestures [35, 54] to subtle motions such as respiration-induced chest movements [47, 52]. In wireless sensing, wireless signals rather than sensors are used for sensing and the contact-free nature makes it appealing in a lot of real-life scenarios.

Diverse wireless signals have been exploited for sensing including Wi-Fi [30, 45], LTE [11, 12, 36], RFID [49, 60], mmWave [15, 26], UWB [54, 56], LoRa [47, 48], sound [24, 44] and Terahertz [4, 16]. While promising in many aspects, several issues still exist in current wireless sensing systems: i) The sensing coverage is still limited. The sensing coverage of one Wi-Fi AP is just a few meters [52]. Although recent studies proposed to use LTE [12] and LoRa signals [47] to extend the sensing coverage to kilometers, it is still much smaller than the coverage of a satellite. Also, around 30% areas are still not covered by LTE stations [17] in the US and this number can be even larger in developing countries. ii) Dedicated sensing signals need to be transmitted which severely affect the original communication function. Take popular Wi-Fi sensing as an example. 100-1000 dedicated packets per second need to be transmitted for sensing [13, 50], which greatly degrade the data rate of ongoing data transmission.

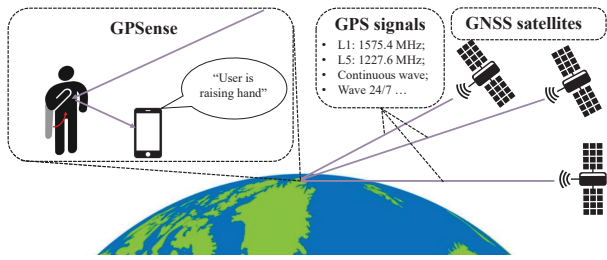


Figure 1: The sensing system based on pervasive and interference-free signals from GNSS satellites.

To address the above challenges, the ideal wireless technology to be exploited for sensing is GPS (Global Positioning System). One GPS satellite can cover 1/8 of Earth and 95% of areas on Earth are covered by at least 4 GPS satellites [10]. Another unique advantage is that GPS satellites continuously emit signals 24/7. Therefore, no dedicated transmissions are required if we utilize GPS for sensing. Surprisingly, we did not find any research utilizing GPS signals for passive sensing (e.g., sensing the human's activities or tracking the human's moving trajectories). Note that passive sensing is different from conventional GPS localization/sensing which is active. While in conventional GPS localization/sensing, a GPS-equipped device needs to move together with the target, GPSense does not require the target to wear/hold a GPS receiver and the GPS receiver is stationary. While promising, multiple challenges need to be addressed before we can use GPS signals for passive sensing.

- The first challenge is that most commercial GPS receiver modules do not report the information required for wireless sensing, i.e., the signal amplitude and phase information. Instead, only carrier-to-noise-density ratio and pseudorange are reported.
- Existing wireless sensing models (e.g., the Fresnel zone model) do not apply to GPS signals due to the extremely long distance between the satellite and target, which is orders of magnitude larger than that of existing sensing modalities. What makes it even more challenging is that GPS satellites move at a high speed with respect to the human target on Earth.¹ In comparison, Wi-Fi AP and LTE towers are stationary with respect to the Earth.
- There are many GNSS (global navigation satellite system) satellites in the Medium Earth Orbit (MEO) and Geosynchronous Earth Orbit (GEO). A GNSS receiver can receive signals from over 30 satellites at the same time from various GNSS satellites including GPS, Galileo (Europe) and BeiDou (China) moving at different speeds. As the navigation satellite moves faster than Earth's rotation, the

satellites a receiver can capture signals from vary during a day. These factors make sensing using GPS signals and more generally GNSS signals more complicated than existing wireless sensing modalities.

To address the first challenge, we propose to reconstruct the original GPS signals including the amplitude and phase from the reported raw measurements at commodity GPS module to enable sensing. However, the reported measurements cannot be directly utilized for signal reconstruction due to inherent errors stemming from satellite movements and atmospheric delay [38]. We apply the measured Doppler shift and satellite ephemeris data publicly available to address the error due to satellite movements. However, after the errors are corrected, fully recovering the original signals is still challenging because the GNSS satellites also modulate encrypted messages on the signals [46]. Fortunately, for sensing, we do not care about the absolute signal amplitude and phase but rather the variation of signal amplitude and phase. As long as the amplitude and phase are stable, we can extract the variations for sensing.

To overcome the second challenge, we leverage the unique long propagation distance of GPS signals to develop the sensing model. Specifically, because of this long transmission distance, GPS signals from the same satellite can be treated as parallel waves with similar signal strengths upon reaching the sensing target and receiver. Building upon this fact, we develop two sensing models for GPS: the diffraction model and the reflection model. For the diffraction model, we adopt the Geometrical Theory of Diffraction (GTD) to analyze the interaction between such parallel signals and the blocking objects (human target). This model is independent of the transmitter location, and the movements of satellites only affect one variable in the model: the incident angle of the signal. This eliminates the need of knowing the transmitter's location in conventional wireless sensing models, which in our case keeps changing, for modelling. The transmitter's location plays a key role in determining the Fresnel zones in the conventional Fresnel zone sensing model [53]. For the reflection model, different from conventional wireless sensing models in which the signals reaching the target and the receiver are non-parallel, the GPS signals reaching the target and receiver can be considered parallel. What is more important is that the signal incident angle reported at the GPS receiver does not change with the target motion because the displacement caused by target motion is too small to change the incident angle owing to the long signal propagation distance. This unique property is utilized to quantify the relationship between signal amplitude/phase variation and target movement.

To address the last challenge, we propose the distributed sensing concept leveraging the large number of satellites

¹The GPS satellite moves faster than Earth's self-rotation.

distributed at different locations on the orbits. We obtain multiple unique observations: i) The signals from satellites located on the *left (right)* side of the human target exhibit better performance for sensing *movements on the left (right) side of the body*; ii) The signals from satellites with *lower elevation angles* achieve a better performance for sensing *the movements of the target's lower body part* (e.g., *gait tracking*). The signals with *higher elevation angles* achieve better performance for sensing *the movements of the target's upper body part* (e.g., *chest movement for respiration monitoring*); iii) As GPS signals are parallel when they arrive at Earth, the signals from satellites on the *same side* of the target with respect to the receiver will be influenced by the target's movements based on the *diffraction* model. Conversely, the signals from satellites on the *opposite side* of the target will be influenced by movements based on the *reflection* model. The information from multiple satellites is further fused to improve the sensing accuracy and robustness.

With all the challenges addressed, we realize GPSense, the first passive wireless sensing system based on GPS signals. Without any hardware modifications, GPSense is able to achieve an accuracy of 94% in recognizing eight human activities. Besides, it can also achieve accurate passive trajectory tracking and respiration monitoring.

We conduct comprehensive experiments to validate the system's robustness under various conditions including different times in a day, different weather conditions, different targets, and diverse environments. We also successfully make the proposed GPS sensing work in indoor environments with the help of a cheap GPS repeater (\$3.5) [1]. GPSense is implemented on multiple mainstream GPS receiver modules used in smartphones and smartwatches. To summarize, we make the following contributions:

- We are the first to harness GPS and more general GNSS signals for passive sensing, wherein the target does not carry a GPS (GNSS) receiver. We believe this new sensing modality enables truly wide-area wireless sensing which will trigger a large range of new sensing applications.
- As sensing just cares about signal amplitude/phase variations rather than the absolute readings, we utilize the reported high-level measurements from commercial GPS modules to reconstruct the GPS (GNSS) signals which are not exactly the same as the original ones but are sufficient for sensing.
- Based on the unique characteristics of GPS signals, we present two sensing models tailored for GPS sensing. These models quantify the relationship between the target movement and corresponding signal variations, laying the theoretical foundation for GPS sensing.
- Based on the unique observations such as the satellites with higher elevation angles are more suitable for sensing

the upper part of the human body, we propose the concept of distributed sensing to fuse signals from multiple satellites to improve the sensing performance.

- We implement GPSense on commercial GPS receiver modules and validate the system's effectiveness and robustness with representative sensing applications (i.e., activity recognition, trajectory tracking, and respiration monitoring) under various conditions. We also show that with a cheap GPS repeater (\$3.5), we can extend GPS sensing to indoor environments.

2 GPS SIGNAL PRELIMINARY

We take GPS as an example to introduce the Global Navigation Satellite System. GPS comprises 31 satellites on the MEO, continuously emitting Radio-Frequency (RF) signals to facilitate navigation functions for billions of devices. Smartphones, drones, and vehicles can receive these signals and determine their positions on Earth through triangulation. The triangulation method requires GPS receivers to receive signals from a minimum of four GPS satellites. Signals from multiple satellites are available nearly anywhere and at any time. Besides, GPS satellites transmit signals at regulated frequency bands (GPS L1 Band at 1575.42 MHz and L5 Band at 1227.6 MHz). Therefore, GPS signals possess the potential as sensing signals for pervasive coverage and at the same time do not affect existing wireless communication signals such as Wi-Fi and LTE.

GPS receiver module embedded in commercial devices, e.g., smartphones, typically only reports important measurements related to localization to optimize computational resource usage and minimize data transmission cost. The most frequently reported measurements are as follows:

Carrier-to-noise-density ratio (C/N_0). This measurement measures the ratio of the power of a signal carrier to the noise power in a 1-Hz bandwidth [22]. This is a key parameter in the analysis of GPS receiver performance. This measurement can be expressed as

$$C/N_0 = 10 \log_{10} \left(\frac{P_c}{P_n/B} \right), \quad (1)$$

where P_c is the power of the GPS carrier, P_n is the power of the noise and B is the bandwidth.

Pseudorange. The pseudorange is a time-of-flight measurement calculated using the *Coarse Acquisition (C/A)-Code*, which corresponds to the distance between the receiver antenna and the satellite antenna, including the receiver and satellite clock offsets and other biases such as atmospheric delays. Pseudorange ρ can be expressed as

$$\rho = r + ct_b + \varepsilon_\rho, \quad (2)$$

where r is the geometric range between the receiver and the satellite, ε_ρ is the measurement error, c is the light speed, and t_b is the clock bias of the receiver.

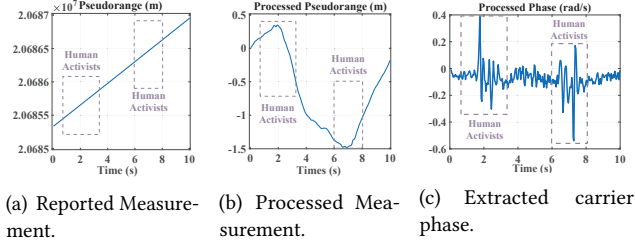


Figure 2: Signal comparison among the reported measurement, processed measurement, and the extracted fine-grained signal phase.

Accumulated Carrier Phase. Commercial GPS receivers can acquire the accumulated carrier phase as a measurement, which keeps accumulating since the GPS receiver starts. The carrier phase measurements Φ can be expressed as

$$\Phi = \frac{r_0}{\lambda} + \int_0^t f_D t dt + \varepsilon_\Phi, \quad (3)$$

where f_D is the frequency shift caused by Doppler effect, r_0 is the initial geometric range between the receiver and the satellite, and ε_Φ is the measurements errors. Note that phase measurements in some GPS receiver systems are reported in meters. For example, Android Smartphones report the carrier phase measurements as *Accumulated Delta Range*, which is actually $\lambda\Phi$.

These measurements play a pivotal role in the navigation application of the commercial device, enabling the computation of its location.

3 GPSENSE MODEL

In this section, we take the GPS signal as an example to illustrate how to reconstruct the original signals based on the reported measurements. Then we present the two sensing models for GPS signals.

3.1 GPS Signal Reconstruction

As mentioned in Sec. 2, the commercial devices can only access the reported measurements from the GPS module, and these measurements can not be directly used for sensing due to multiple reasons: i) Measurement errors. Errors are caused by various factors such as weather and clock drift during the long-range (about 20,000 km) propagation. The signal variation caused by the sensing target can be buried in the variation caused by errors without being detected. ii) Coarse channel state information: the measurements are reported for calculating the distance between satellites and the receiver and the measurements are too coarse to be utilized for fine-grained sensing (e.g., respiration monitoring). To extract the fine-grained channel state variation for sensing, we design a *signal reconstruction scheme* to reconstruct the original GPS signals using the reported GPS measurements.

Measurement error correction. In this step, we preprocess the GPS-reported measurements to eliminate errors during the long-range propagation. Specifically, there are two factors that cause errors in the GPS measurements: i) movements of the satellite; and ii) clock error of the GPS receiver. These factors should be addressed properly to reduce their influence on sensing.

First of all, to eliminate the influence of GPS movements, we exploit the publicly accessible ephemeris data, which reports the locations of the satellites. We use the satellite's location and orbit information to estimate the movement status of each satellite. After we obtain the movement status of the satellite, we calculate the effect of the Doppler frequency shift on the signal phase caused by the movement, and then we compensate the phase error caused by Doppler frequency shift (f_D) in the accumulated carrier phase measurements. To mitigate the effect of clock errors on pseudorange (t_b), we employ the weighted least squares method [22]. This method involves multiple synchronized satellites to calculate the clock bias between the satellites and the receiver, enhancing the precision of the measurements [29].

Basic signal parameter calculation. In the second step, we combine these pre-processed measurements to calculate the basic signal parameters, i.e., amplitude $Amp(t)$ and phase $\phi(t)$. Then, the GPS signal is reconstructed for sensing. $Amp(t)$ can be estimated as

$$Amp(t) = \sqrt{P_n 10^{(C/N_0)/10}}, \quad (4)$$

where $P_n = kT$ is the noise power in a 1-Hz bandwidth [22], k is the Boltzmann constant in Joules per Kelvin, T is the temperature in Kelvin, and C/N_0 is the reported Carrier-to-noise-density ratio. The carrier phase ϕ of the GPS signal can be expressed as

$$\phi(t) = 2\pi \left(\frac{d\Phi}{dt} - f_D t + \frac{\rho - ct_b}{\lambda} \right), \quad (5)$$

where Φ is the reported accumulated carrier phase, ρ is the reported pseudorange, f_D is Doppler frequency shift caused by the satellite movement, t_b is the clock bias of the receiver. After obtaining the amplitude and phase values, we can reconstruct the GPS signal at timestamp t as

$$S(t) = Amp(t) e^{j\phi(t)}. \quad (6)$$

To demonstrate the sensing capability of the reconstructed GPS signal, a benchmark experiment is conducted, wherein a human target is asked to move around the GPS receiver module, inducing variations in the received signals. Figure 2 depicts the reported pseudorange, the corrected pseudorange and the reconstructed signal phase. It is evident that the reported pseudorange does not contain meaningful information due to the aforementioned measurement errors. Moreover, even with the correction of the reported pseudorange, its signal variation fails to show the fine-grained channel changes induced by the target's movement around

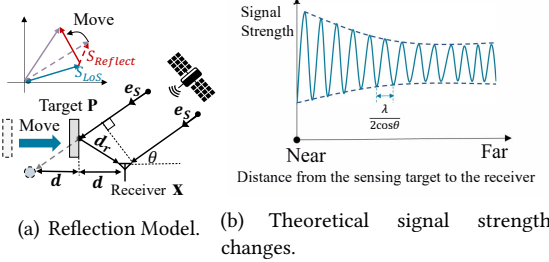


Figure 3: A sensing target moves away from the LoS path between the satellites and the GPS receiver.

the receiver, as the pseudorange measurement is designed for coarse-grained distance estimate. Ultimately, our proposed method successfully yields fine-grained signal phase variations caused by the target's movement. Without loss of generality, we employ the reconstructed signals to represent the received GPS signals in subsequent sections for sensing. Besides, the reconstruction process is similar for other GNSS satellites such as BeiDou.

3.2 The Reflection of GPS Signals

After reconstructing the GPS signals from the reported measurements, we proceed to establish the correlation between signal variations and target movements for sensing. The conventional sensing models, e.g., the Fresnel zone model [53], are not suitable for GPS signals due to the extremely long signal propagation distance and constantly moving satellite at a speed of about 4 km/s. In this section, we model the reflection of GPS signals and quantify the relationship between target movements and the induced signal variations. We analyze the model theoretically and validate its effectiveness through experiments.

Modeling the reflection from a moving object. In this section, we focus on the reflection model for moving objects. As shown in Figure 3, a target moves away from a receiver. The receiver captures signals from the LoS path and the reflection path d_r from the target. The horizontal distance (d) from the GPS receiver to the target can be expressed as

$$d = d_r \cos \theta, \quad (7)$$

where θ is incident angle of the GPS signal. Then the phase difference between the LoS signal S_{LoS} and reflection signal $S_{Reflect}$ can be simplified as

$$\phi_{Reflect} - \phi_{LoS} = \frac{4\pi d \cos \theta}{\lambda} + \pi, \quad (8)$$

which is linearly related to the distance d as the elevation angle of the satellite is a constant in a short time window (e.g., 10 s). Due to the constructive and destructive combination between the LoS signal and the reflection signal illustrated in Figure 3(a), the signal will manifest repetitive peaks during

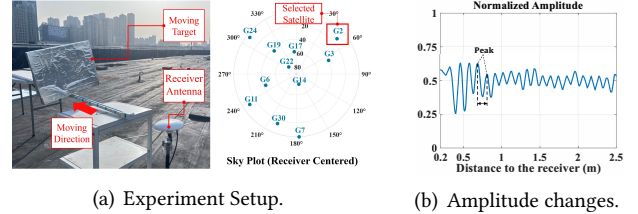


Figure 4: Reflection Verification Experiment: a metal box moves away from the GPS Receiver.

the process of target movement, as demonstrated in Figure 3(b). Based on Equation 8, we know the interval between adjacent two peaks is $\frac{\lambda}{2 \cos \theta}$, allowing us to deduce the distance of the target's movement by measuring the number of observed peaks. The peak signal strength decreases as the target moves further away from the receiver.

We conduct a benchmark experiment to verify the theoretical observation. We place a metal box on a sliding rail and move it away from the receiver. We then measure the distance between two adjacent peaks to validate our model. As shown in Figure 4 (b), We plotted the measured GPS signal strength from satellite G19. The average of measured moving distances between two peaks is 0.105 m, which matches the theoretical distance (0.101 m) based on Equation (8). For this reflection model, only the reported signal incident angle is required for sensing without a need of knowing the satellite's detailed status such as moving speed and position.

Reflection from the human body. In the reflection model, the received signal contains both the reflection signal and LoS signal. However, due to weaker signal (-120 dBm) compared to other wireless signals such as Wi-Fi, the GPS reflection signal can only be detected when reflected from a relatively large body part, such as the torso. The weaker reflection signals from arms are hard to be detected. To sense arms and legs, signals from other satellites which are influenced by the diffraction effect can be used. Detailed results of experiments on tracking, localization, and activity detection will be presented in § 5.

3.3 The Diffraction of GPS Signals

In this section, we present the diffraction model for GPS sensing to quantify the effect of motion activities on signal variations. Both theoretical analysis and experiment are employed to validate the proposed model.

Modeling the diffraction effect caused by a moving object. The diffraction effect dominates when the human target is very close to or on the LoS path of the GPS signal. When a GPS signal wave impinges on the edge of an object (e.g., a human target), Keller's Geometrical Theory of Diffraction

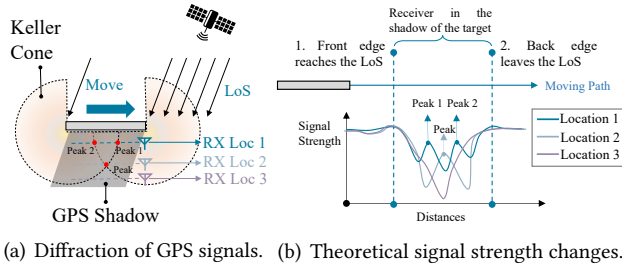


Figure 5: A sensing target moves across the LoS path between the satellites and the GPS receiver.

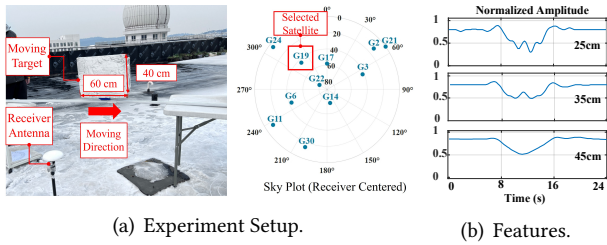


Figure 6: Diffraction Verification Experiment: a metal box moves across the LoS path between the GPS Reiever and a GPS satellite.

(GTD) [20] depicts that the occurrence of outgoing rays is in the shape of a cone. In this work, we focus on the case of moving objects for sensing.

As shown in Figure 5 (a), considering a scenario that a target moves across the LoS path between a GPS satellite and a GPS receiver, GPS signals get diffracted at the edge of the moving target. When the target moves further, the object's Keller Cone due to diffraction appears. Now the GPS receiver receives a combination of the diffracted signals and the LoS signals, causing a small variation of the combined signal strength as the LoS path signal still dominates. When the target moves further and the LoS path is obstructed, the strength of the received signal decreases rapidly. During the process of moving across, the signal strength fluctuates. As shown in Figure 5, when a GPS receiver is located at different locations, the signal strength fluctuation pattern varies. When the GPS receiver is deployed at Location 1, two peaks appear on the signal strength plot during the process of moving across the LoS path. When the receiver is at Location 2, only one peak appears. At Location 3, due to destructive combination, only one valley can be observed.

We conduct an experiment to see the signal variation when an object moves across the LoS path between the satellite and the GPS receiver. As shown in the Figure 6(a), we employ a metal box as the object and the G19 satellite as the transmitter. The elevation angle of the satellite is about 43

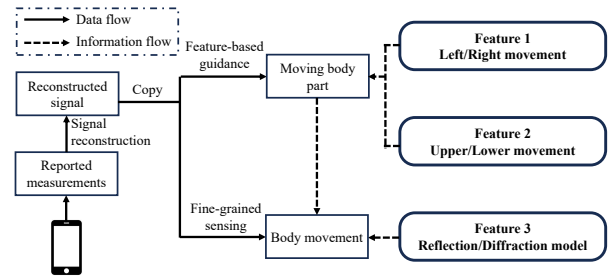


Figure 7: System pipeline

degrees. When we place the GPS receiver at a distance of 25 cm, 35 cm and 45 cm away from the target moving trajectory, we obtain three plots (i.e., two peaks, one peak and one valley) as shown in Figure 6(b) which match the theoretical analysis in Figure 5 well.

The diffraction of the human body. The human body causes rich diffraction when the body is near to or on the LoS path [53]. Based on the analysis and experiments in previous sections, the GPS signal variation pattern can be leveraged to infer the motion of the target. The target movement directions can also be acquired when we employ multiple satellites for sensing, which will be detailed in § 4.

4 GPSENSE DESIGN

So far, we have established the basic sensing model for the proposed system based on the GPS signals from a single satellite. There are over one hundred GNSS satellites currently in use, including GPS, BeiDou, etc. The signals from all these satellites can be utilized for our sensing tasks. This brings the concept of distributed sensing and we leverage signals from multiple satellites to improve the sensing performance in terms of sensing accuracy and sensing robustness. As signals from multiple GNSS satellites in the MEOs can be concurrently received, it is thus important to dynamically select proper satellites as the signal sources for sensing. In this section, we also introduce the unique features of GPS signals and leverage them for sensing. The signal processing pipeline is presented in Figure 7.

4.1 Sensing with Multiple Satellites

Based on the two sensing models introduced in § 3, we pinpoint three features regarding the sensing capability of GPS signals related to satellite positions. Benchmark experiments are employed to validate the identified features.

Feature 1: Satellite on the right/left of the target. The first factor influencing the GPS signal's sensing capability is the azimuth direction of the satellite. Based on the established sensing models, signals transmitted from satellites positioned to the right of the target have a higher probability of undergoing diffraction/reflection effects caused by

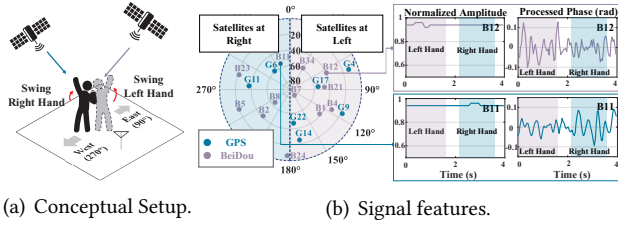


Figure 8: Combine the GNSS signals from satellites at different azimuth angles.

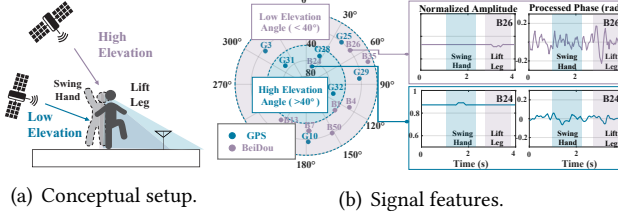


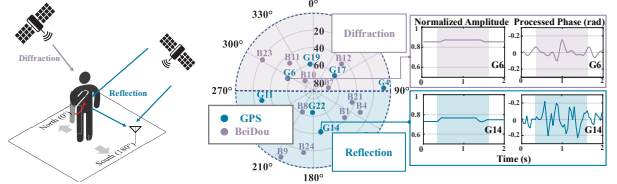
Figure 9: Combine the GNSS signals from satellites at different elevation angles.

the right side of the body. Consequently, variations in these signals contain more information of movements on the right side of the target. As shown in Figure 8, signals emitted from satellites located on the *right side* of the target exhibit superior sensing capability for *movements on the right side of the body*. Similarly, signals from satellites positioned on the *left side* can better sense *movements on the left side of the body*.

As depicted in Figure 8(a), the target faces the GPS receiver in the direction of 180° (South). The target first waves her left hand and then waves her right hand. Figure 8(b) displays the sky plot at the specified timestamp and the signal variations from satellite B12, positioned to the left of the subject, and satellite B11, positioned to the right of the subject. It is evident that when the subject swings her left hand, it solely affects the signals from satellites positioned to her left, and similarly when swinging her right hand. As plotted in Figure 8(b), both amplitude and phase are affected significantly by the subject's gestures.

Feature 2: Satellite at high/low elevation angle. Another feature influencing the sensing capability of GPS signals is the elevation angle. As illustrated in Figure 9(a), signals from satellites with *higher elevation angles* show superior sensing capability for *upper body movement*, whereas signals from satellites with *lower elevation angles* excel in sensing *lower body movement*.

We conduct an experiment to validate this feature, as depicted in Figure 9(a), where the subject first swings her hand and then lifts her leg. The amplitude and signal phase variations during the process of the movements are shown in Figure 9(b). When the subject swings her hands, the signals from a satellite at a high elevation angle (B24) experience significant influence, while signals from a satellite at a low



(a) Conceptual setup. (b) Signal features.

Figure 10: Combine the reflection and diffraction GNSS signals for sensing.

elevation angle (B26) remain relatively stable. This suggests that the upper body of the subject is in motion while the lower part remains static. Similarly, the movement of lifting leg tends to affect the GPS signals from a satellite with a lower elevation angle (B26) rather than a satellite with a higher elevation angle (B24).

Feature 3: Satellite at same/opposite side of the target.

Due to the extremely long transmission distance of GPS signals, GPS signals are parallel when they arrive at the target and receiver. When the satellite and the target are at the *same side* with respect to the receiver (Satellites in the north in Figure 10), GPS signals will be influenced by *diffraction*. When the satellite and the target are at the *opposite side* with respect to the receiver (Satellites in the south in Figure 10), the signal variation is caused by *reflection*.

We conduct an experiment to validate this feature. The experiment setup is depicted in Figure 10(a), where the subject puts her hand on the chest and then puts it back. We plot the satellite sky plot during the experiment and the amplitude and phase variations from two selected satellites, namely G6 and G14 as shown in Figure 10(b). Based on the geo-location relationship, the diffraction model should be applied for G6, and the reflection model should be applied for G14. As depicted in Figure 10(b), both models can sense the target's motion. This shows the capability of the proposed system to employ both models for concurrent sensing.

4.2 Feature-based sensing design

Based on the described features, we propose to combine these features for device-free activity recognition. While we employ activity recognition to illustrate the concept, our system can be applied for other sensing applications such as respiration monitoring and device-free trajectory tracking which will be demonstrated with experiments in § 5.

A GPS receiver can receive GPS signals from multiple satellites in the sky. We can thus generate a sky plot as depicted in Figure 11 (left). Then, we identify which part of the target's body is moving by comparing signal strength variations caused by target movement at different satellites using Feature 1 and 2. Take one target swinging her left hand as the example. We first compare the average signal variation from satellites on the left side with that from the right side.

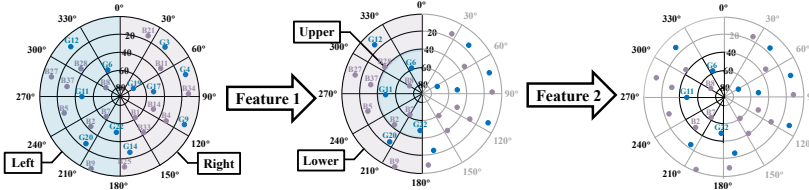


Figure 11: Select satellites based on Feature 1&2.

If the value from the left side is higher, our system concludes that the movement is from the left side of the target, and vice versa. In the current scenario, with larger left-side signal variations, we only consider GPS signals from the left side as shown in Figure 11. Similarly, the system further compares the average signal variation at high-elevation angles with that at low-elevation angles. The elevation angle threshold is set as 40 degrees as illustrated in Figure 11. We observe that the average signal variation at high-elevation angles exceeds that at low-elevation angles. The system thus deduces that the current movement pertains to the upper body part of the target based on Feature 2.

4.3 Fine-grained Activity Sensing

We employ dynamic time warping (DTW) to compare the collected signal templates with the reference templates stored in the database for fine-grained activity recognition. However, the crucial aspect lies in how we combine GPS signals from multiple remaining satellites after the feature-based selection for sensing. We still employ the example of a target swinging her left arm to illustrate the concept. For reference (database) signal collection, the target is only required to perform the movement once as the collected GPS signal contains data from all satellites present in the sky at that specific timestamp.

Combining the reflection and diffraction models. After we know the basic information of the movement (e.g., left-side upper-body movement), we can apply Feature 3 to tell if the signal from a particular satellite experiences a diffraction effect or reflection effect. The reference template for each movement based on the diffraction model is denoted as $X^D(i)$, where $i \in N$ and N represents the set of left-side upper-body movements. Similarly, the reference template for each movement based on the reflection model is denoted as $X^R(i)$, where $i \in N$. We then select the current template to be classified by identifying the received GPS signal with the largest variation. The current template is designated as x^D for the diffraction model and x^R for the reflection model. The dynamic time warping (DTW) method is applied as:

$$\arg \min_{i \in N} ||x^D||^2 \mathbf{DTW}(x^D, X^D(i)) + ||x^R||^2 \mathbf{DTW}(x^R, X^R(i)). \quad (9)$$

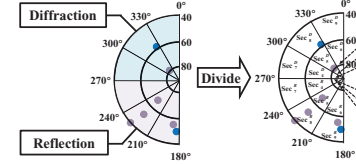


Figure 12: Combine two models and sector division.

Here, $||x^D||^2$ and $||x^R||^2$ represent the signal variance for the current template based on the diffraction and reflection models, respectively. They are multiplied as weights to the corresponding DTW results, which represent the contribution of the reflection and diffraction models for sensing.

However, the GNSS satellites are constantly moving. Although we have compensated for the influence of the satellite movement on signals in § 3, the satellite positions during the collection of the current template differ from those during the collection of the reference template. Even for the same movement, GPS signal variations for satellites at different positions are distinct. Thus, the signal variations depend not only on target movement but also on the satellite's positions, rendering the basic DTW method ineffective.

To address this issue, we leverage the observation that *the signal variations for satellites within an azimuth and elevation angle range exhibit similar patterns for the same target movement*. Based on our experiments, the angle range is 30 degrees for the azimuth angle and 20 degrees for the elevation angle. Thus, we subdivide the sky plot into smaller sectors based on these azimuth and elevation angle ranges as shown in Figure 12. This ensures that within the same angle sector, the signal patterns of different satellites for the same target movement remain consistent.

When collecting the reference template for a specific movement, we divide satellites based on angle sectors and select the template with the largest signal variations in each sector, denoted as $X_j^R(i)$ and $X_j^D(i)$, where $j \in M$, $i \in N$, and M represents the set of sectors. Note that the user is required to perform each movement only once for reference template collection. Additionally, we allocate a weight to each sector, where the weight for each sector is denoted as $W_j^R(i)$ and $W_j^D(i)$ ($j \in M$, $i \in N$) based on signal variations. While the current template is a set of signals with the largest variations in different sectors as x_j^R and x_j^D , where $j \in M$. The complete algorithm to classify the current template as the specific movement is presented below:

$$\begin{aligned} \arg \min_{i \in N} & \sum_{j \in M} ||x_j^D||^2 W_j^D(i) \mathbf{DTW}(x_j^D, X_j^D(i)) \\ & + \sum_{j \in M} ||x_j^R||^2 W_j^R(i) \mathbf{DTW}(x_j^R, X_j^R(i)). \end{aligned} \quad (10)$$



Figure 13: GNSS Module.

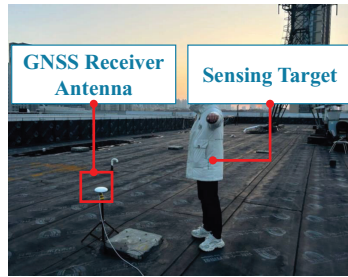
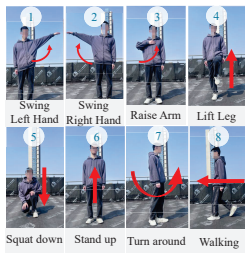
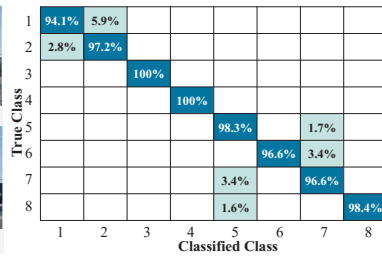


Figure 14: Default setup.



(a) Activities.



(b) Accuracy.

Figure 15: Overall human activities sensing accuracy.

5 EVALUATION

5.1 Implementation

In this section, we introduce the implementation of GPSense. As depicted in Figure 13, we use the Ublox F9P GNSS module as the default receiver with an update rate of 25 Hz. We test GPSense on various commercial GNSS receivers with update rates ranging from 1 Hz to 25 Hz to confirm its broad applicability. For processing signals, we employ a laptop equipped with an Intel i7 CPU and 16 GB of memory. The default setup, as depicted in Figure 14, is simple: a GNSS receiver is positioned on the ground or roof while the target performs activities or moves around nearby.

5.2 Human Activity Sensing

In the first experiment, we ask a volunteer to perform eight different body movements as shown in Figure 15(a) to evaluate GPSense's sensing accuracy for human activities. For each activity, the target repeats the movement 100 times, while we take one of the templates as the reference. Figure 15 shows that the sensing accuracy for these eight activities is about 97.6%. Moreover, we notice that some activities such as raising the arm cause changes on both reflection and diffraction features. This observation supports our approach of combining reflection and diffraction models for sensing.

Sensing with different GNSS receiver modules. As depicted in Figure 16(a), we implement GPSense on multiple different commercial GNSS receiver modules, receive both



(a) Sensors.

True Class	1	2	3	4	5	6	7	8
Classified Class	1	2	3	4	5	6	7	8
1	92.4%	3.8%	3.8%					
2	3.3%	93.5%	3.3%					
3			100%					
4				2.9%	97.1%			
5					1.8%	98.2%		
6						100%		
7							0.9%	
8								97.4%

(b) U-blox M10.

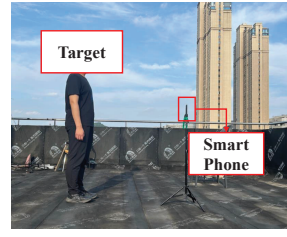
True Class	1	2	3	4	5	6	7	8
Classified Class	1	2	3	4	5	6	7	8
1	94.3%	2.9%	2.8%					
2	1.9%	98.1%						
3	3.8%	3.9%	92.3%					
4				100%				
5					100%			
6						100%		
7							5.3%	
8								94.7%

(c) U-blox M9N.

True Class	1	2	3	4	5	6	7	8
Classified Class	1	2	3	4	5	6	7	8
1	94.3%	2.9%	2.8%					
2	1.9%	98.1%						
3	3.8%	3.9%	92.3%					
4				100%				
5					100%			
6						100%		
7							5.3%	
8								94.7%

(d) U-blox M8N.

Figure 16: Sensing accuracy with different GNSS receiver modules.



(a) Experiment Setup.

True Class	1	2	3	4	5	6	7	8
Classified Class	1	2	3	4	5	6	7	8
1	96%	0%	4%	0%	0%	0%	0%	0%
2	4%	96%	0%	0%	0%	0%	0%	0%
3	6%	0%	94%	0%	0%	0%	0%	0%
4	0%	0%	0%	96%	0%	12%	2%	0%
5	0%	0%	0%	0%	90%	0%	0%	10%
6	0%	0%	0%	0%	0%	100%	0%	0%
7	0%	0%	0%	0%	2%	0%	90%	8%
8	0%	0%	2%	4%	0%	4%	0%	90%

(b) Accuracy.

Figure 17: GPS sensing with a smartphone.

GPS and BeiDou signals, and conduct experiments to evaluate their performance. These modules are commonly found in smartwatches (e.g., Ublox M10 [2]), smartphones (e.g., Ublox M9N [39]), robots, and unmanned aerial vehicles (e.g., Ublox M8N [40]). In each experiment, the target repeats the same eight activities as in the previous section with each GNSS receiver modules. These modules operate at the default sampling rate of 10 Hz, 25 Hz, and 15 Hz to collect GNSS signals, respectively. The corresponding sensing results are presented in Figure 16(b), Figure 16(c), and Figure 16(d), with an average sensing accuracy of 97.3%, 97.2%, and 97.4%, respectively, which are similar to the sensing accuracy of the default GNSS receiver (97.6%). These results demonstrate that our system can work on various commercial GNSS receiver modules.

Sensing with commodity smartphones. We implement GPSense on a commodity smartphone (Google Pixel 4), and conduct experiments to evaluate the performance. As shown in Figure 17, we fix the smartphone on a tripod and ask a volunteer to stand in front of it. The volunteer repeats the eight body activities defined in Figure 15(a) and the smartphone records the GNSS readings with an open-source GNSS data logger [14]. For the smartphone, the sampling rate of the GNSS readings is only 1 Hz. We apply the Cubic Spline Interpolation scheme, which is lightweight and can smoothly

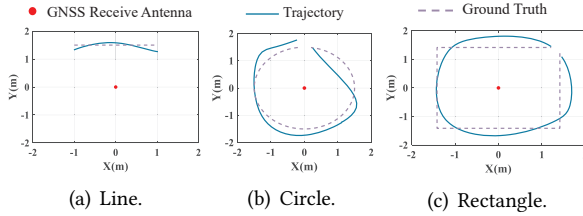


Figure 18: Passive trajectory tracking.

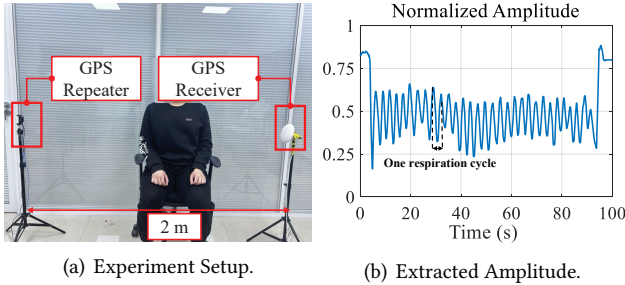


Figure 19: Indoor respiration sensing.

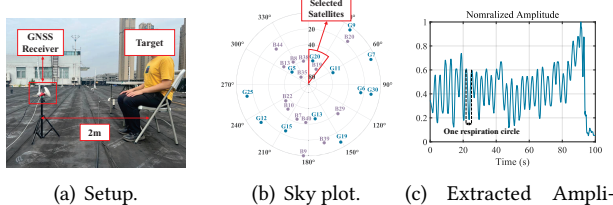


Figure 20: Outdoor respiration sensing.

approximate data points, to increase the sampling rate of the smartphone-recorded data to 25 Hz. The achieved activity recognition accuracy is 92.75%, which is lower than that achieved with the U-blox M10 module (97.2%). We believe this is mainly due to the much lower sampling rate (1 Hz vs. 25 Hz). This result is still good enough to show that GPSense can be deployed on smartphones.

5.3 Passive Trajectory Tracking

In addition to activity sensing, our system can also passively track the trajectory of the target near the GNSS receiver. Our system does not require the target to carry a GNSS receiver. Instead, it obtains the trajectory by analyzing signal variations caused by the target moving. We ask a volunteer to walk along the pre-defined trajectories including a straight line, a circle and a rectangle near the GNSS receiver as shown in Figure 18(a). The key principle behind trajectory tracking is that the human's walk affects the LoS paths of different satellites temporally. By combining readings from many satellites, our system can achieve decimeter-level passive trajectory tracking, as shown in Figure 18.

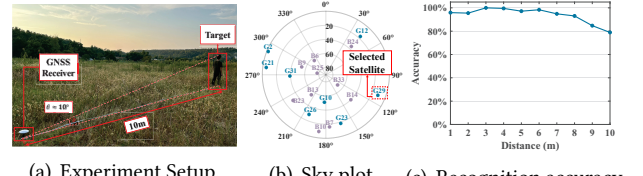


Figure 21: The recognition accuracy under different sensing distances.

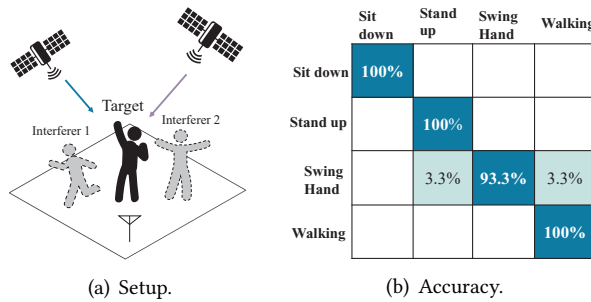
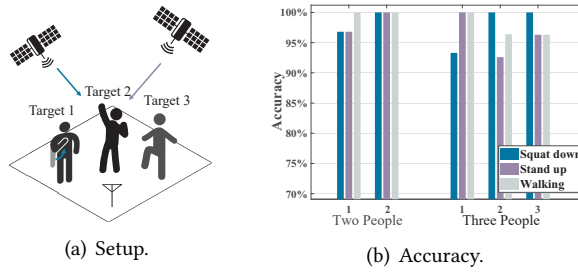
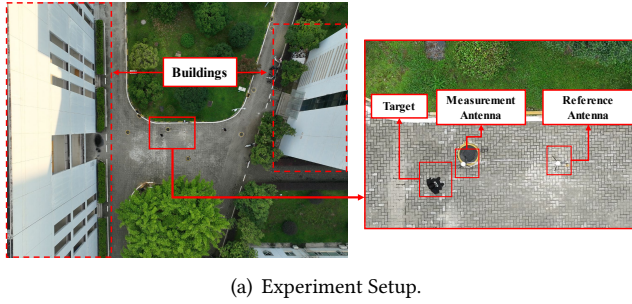
5.4 Contact-free Respiration Monitoring

The proposed system can also be used to monitor subtle vital signs of the target, i.e., respiration. Since respiration monitoring typically happens in indoor environments, we employ a low-cost GNSS repeater (\$3.5) to bring GNSS signals into the room [9]. The experiment setup is illustrated in Figure 19(a), where the repeater is deployed 2 m away from the GNSS receiver. Then we ask a volunteer to sit between the GNSS repeater and the receiver. We instruct the user to breathe naturally 30 times and use the GNSS receiver to collect signals during the process. The extracted signal amplitude variations based on the proposed signal reconstruction method, are plotted in Figure 19(b). We can see that each peak-valley pair corresponds to one respiration cycle, with 30 peaks and valleys clearly observed. Furthermore, we instruct the volunteer to breathe naturally for 90 seconds and count the number of breath cycles. We repeat the experiment ten times. The achieved average respiration rate estimation error is 0.6 beats per minute (bpm), which falls in the category of good performance [51].

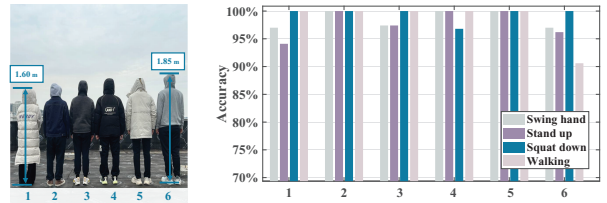
Respiration monitoring outdoors. We place the GNSS receiver on the roof and ask the volunteer to sit in front of it, as shown in Figure 20(a). As illustrated in Figure 20(b), we utilize two satellites (i.e., GPS G20 and Beidou B19) and combine the received signals to extract chest movement. The extracted signal amplitude is plotted in Figure 20(c) with each peak-valley pair corresponding to one respiration cycle. We instruct the volunteer to breathe naturally for one minute and count the number of breath cycles. We repeat the experiment ten times. The overall respiration rate estimation error is 0.57 bpm, demonstrating the effectiveness of using GNSS signals for respiration sensing in outdoor environments without the need for GPS repeaters.

5.5 Sensing Capabilities

In this section, we explore the performance boundary of GPSense, including the sensing coverage and multi-target sensing. We choose four representative human activities, i.e., walking, vertical hand movement, sitting down, and standing up for the following experiment.

**Figure 22: One target and two interferers.****Figure 23: Three targets.****Figure 24: The sensing accuracy near tall buildings.**

Sensing coverage. In this experiment, the volunteer is asked to perform activities at various distances away from the GNSS receiver, as shown in Figure 21(a). The main factor limiting the coverage is the elevation angle of selected satellites, where a lower elevation angle tends to have a larger sensing coverage. Therefore, we select a satellite with a low elevation angle (about 10 degrees) to evaluate the maximum

**(a) Various targets.****(b) Sensing Accuracy.****Figure 25: The sensing accuracy under different target sizes.**

sensing coverage. The achieved sensing accuracy at different distances is presented in Figure 21(c). The accuracy decreases with the distance as the signal strength decreases. However, a reasonably high accuracy (i.e., 93.1%) can still be achieved at a distance of 8 m.

Sensing multiple persons. We further evaluate the performance of our system in multi-target sensing. We ask three volunteers to participate in two multi-target scenarios with different sensing purposes. For the first scenario, our system recognizes the activity of one volunteer while considering the other two as interferers. The interferers randomly move as shown in Figure 22(a). The achieved average sensing accuracy is 98.3% as shown in Figure 22(b). Due to a large number of satellites (usually 20-30) available, there always exist GPS signals that are influenced only by the target and not by the interferers. Our system utilizes these clean signals to mitigate the influence of surrounding interferers on sensing.

In the second scenario, all three volunteers are targets. We ask the three volunteers to simultaneously perform activities as illustrated in Figure 23(a), and the sensing performance is shown in Figure 23(b). The average recognition accuracy is 98.9% when two volunteers concurrently perform gestures. The average accuracy decreases slightly to 97.2% when three volunteers concurrently perform gestures. Large number of distributed satellites enable our system to pick signals only affected by one single target, making multi-target sensing possible.

Impact of multipath. We conduct experiments between two tall buildings to evaluate the performance of GPSense in rich-multipath environments, as shown in Figure 24(a). To address performance degradation caused by multipath, we propose a differential sensing scheme using two GNSS receivers. For comparison, we first performed experiment with a single GNSS receiver. The results, shown in Figure 24(b), indicate a significant drop of performance (an average accuracy of 76.9%) in the presence of tall buildings. To address this issue, we introduce a second receiver as a reference and employ the differential operation between the two receivers. The results, depicted in Figure 24(c), demonstrate a substantial improvement of accuracy (an average accuracy of 88.9%).

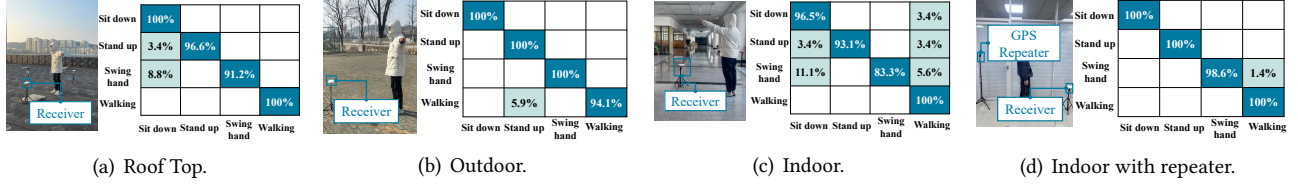


Figure 26: The sensing accuracy at different locations.

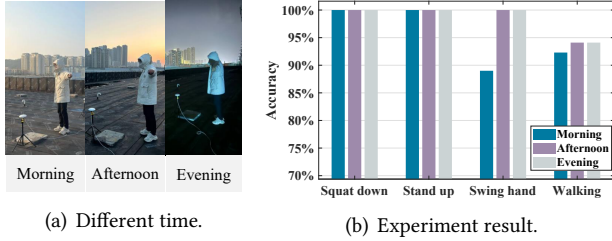


Figure 27: The sensing accuracy at different times.

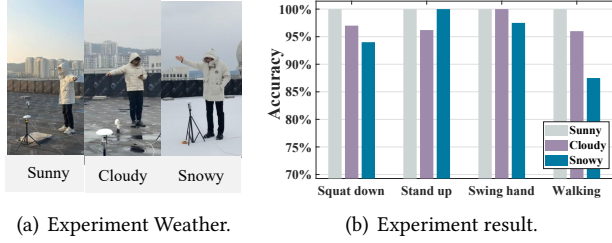


Figure 28: The sensing accuracy in different weathers.

5.6 System Robustness

In this section, we evaluate the robustness of the proposed system against target variations, diverse experiment environments (both indoor and outdoor), different times of a day, and various weather conditions. Similar to the previous experiment, we select four representative human activities for recognition.

Impact of human diversity. Based on the proposed models, the size of human target may influence the system performance. We conduct experiments involving six volunteers with heights ranging from 160 cm to 185 cm, as detailed in Figure 25(a) to repeat the four activities: walking, vertical hand movement, sitting down, and standing up near the GNSS receiver. Each volunteer repeats each activity 50 times, and we use one template of each movement collected from the 180 cm volunteer as the reference template for all targets. The sensing accuracy for each target is detailed in Figure 25(b), from which we can observe slight variations across targets. The overall accuracy for all targets remains high (98.6%).

Sensing at different places. One advantage of our system is that the pervasive GNSS signals are accessible almost everywhere on Earth. We choose four different experiment

environments: a rooftop, an outdoor park, an indoor space with open windows (weak GNSS signals as noted in [58]), and a confined room equipped with a GNSS repeater, as shown in Figure 26, to evaluate the sensing performance. In each environment, we instruct a volunteer to repeat the four different activities 50 times. As shown in Figure 26, the average sensing accuracies for the four environments are 97.0%, 98.5%, 93.2%, and 99.7%, respectively. The sensing accuracy in the third environment, i.e., indoor with window-leaked GPS signals, is slightly lower. This is because the building obstructs most of the GNSS signals. To enhance the sensing capability of our system in indoor environments, we can deploy a low-cost GNSS repeater as demonstrated in the fourth scenario.

Impact of different time. Another advantage of GPSense is that GNSS satellites transmit signals 24/7, ensuring that the system's sensing service is accessible any time. As illustrated in Figure 27(a), the volunteer is instructed to perform four different activities at three different times during the same day. We take one template of each movement in the afternoon as the reference template for all the tests. The experiment results are presented in Figure 27(b), from which we observe slightly different sensing accuracies at different time (95.3%, 98.5%, and 98.5%). Since a large number of satellites are available at any point of time, the sensing performance generally remains stable over time. However, performance degradation does sometimes occur due to signal quality variations.

Impact of weather condition. Different from wireless signals used in existing sensing systems, such as Wi-Fi, GNSS signals are influenced by weather conditions due to the extremely long transmission distances. Thus, we test the influence of different weather conditions on the performance of our system. As illustrated in Figure 28(a), the volunteer performs four different activities under three different weather conditions: sunny, cloudy, and snowy. We take one template of each movement under the sunny weather as the reference template for all the tests. Figure 28(b) shows the corresponding experiment results, and the average sensing accuracy under the three weather conditions is 100%, 95.9%, and 94.7%. These results indicate that weather condition does slightly affect the sensing performance and best performance can be achieved in sunny days.

6 DISCUSSION

Comparison with sensing using other ambient signals.

Employing GNSS signals for sensing exhibits the following advantages: i) GNSS has a wider coverage while FM [37], TV [34], and LTE signals [6, 11, 12] do not cover some rural areas; ii) A GNSS receiver can usually receive signals from eight or more distributed GPS satellites in various directions. This provides rich spatial diversity for sensing which other wireless signals cannot provide; iii) Since a smartphone contains both GNSS and other wireless modules, different wireless sensing modalities can be fused for even better sensing performance; iv) The more accurate synchronization capability presents GPS sensing with the advantage of fusing information from different satellites for distributed sensing.

Other satellites. We assess the performance of our system across various GNSS satellites, including BeiDou and Galileo. Remarkably, our findings indicate negligible performance differences when utilizing signals from different navigation systems, demonstrating the system's robustness. In addition to GNSS satellites, various other satellites, including communication satellites like Starlink and TV satellites, also continually transmit wireless signals to Earth. We believe these signals also have the potential to be utilized for sensing.

Limited Number of Activities. The current system only leverages very basic signal processing methods such as Dynamic Time Warping (DTW) for activity classification. We believe that incorporating machine learning-based classification models could increase the number of activities the system can recognize.

7 RELATED WORK

Wireless sensing. In recent studies, researchers employ wireless signals, including Wi-Fi [18, 42], UWB [21, 54], and sound [24, 55], for diverse sensing applications. These applications include contact-free activity recognition [35], vital signs monitoring [41], and passive localization [25]. However, a majority of sensing systems require a dedicated signal transmitter, such as mmWave [59], or adversely impact the original communication function, exemplified by Wi-Fi [50]. To remove the need of dedicated sensing signals, approaches are explored such as leveraging signals emitted from LTE towers [11] and signals leaked from power lines [8] for sensing. For the first time, GPSSense utilizes the pervasive signals emitted from GNSS satellites for wireless sensing, which eliminates the need for a dedicated signal transmitter and avoids interference on communication.

GPS technologies. GPS signals are originally designed to provide global positioning services. Billions of devices rely on GPS signals for localization [23]. Recent efforts are mainly devoted to enhancing the accuracy and coverage of GPS [5, 9, 28, 29, 58]. Besides their primary function for

positioning and navigation, researchers also harness GPS signals for remote sensing and mapping, including atmospheric monitoring [19, 43] and driver behavior analyzing based on GPS records [57]. Different from conventional approaches, our approach utilizes the GPS signal itself as a sensing tool to passively sense the motion information of the target.

GPS tomography. GPS tomography technologies [3, 33] also employ GPS signals to sense targets [33] and vapor distribution [3] by analyzing the signal delays. Unlike approaches that directly measure propagation delay using GNSS raw data, our method achieves fine-grained sensing by analyzing the changes in both line-of-sight (LoS), diffracted, and reflected signals. This analysis is based on reconstructed GPS signals instead of the raw measurements.

Diffraction model. The Keller Geometrical Theory of Diffraction (GTD) elucidates the diffraction phenomenon arising when an energy wave impinges upon an object edge [20]. Notably, recent research endeavors involve the design of a metasurface composed of small metal plates functioning as diffraction edges to exert control over RF signals, aligning with the principles of the Keller Cone [31]. Furthermore, researchers employ the diffraction model for the purpose of recognizing letter objects placed behind a wall using RF signals [32]. In contrast to existing works, our approach utilizes the diffraction model to analyze the influence of moving objects on GPS signals for sensing.

8 CONCLUSION

In this work, we introduce the very first wireless sensing system based on GPS (GNSS) signals from satellites. By reconstructing the signals based on reported measurements from commercial GNSS receivers, we make GNSS signals for sensing possible. Two sensing models are established based on the unique property of GNSS signals, i.e., the extremely long transmission distance. We further propose the concept of distributed sensing to fuse GNSS signals from multiple satellites to improve sensing performance. GPSSense was implemented and evaluated on commercial GNSS receivers. We believe the proposed new sensing modality can inspire a large spectrum of sensing applications utilizing distributed satellites in space.

ACKNOWLEDGEMENT

We thank the anonymous shepherd and reviewers for their insightful comments, which greatly improved the quality of the paper. This work was supported by the National Natural Science Foundation of China with Grant 62071194 and 62471194, the Fundamental Research Funds for the Central universities.

REFERENCES

- [1] Alibaba. 2024. Car Mobile Navigation GPS Signal Enhancement Amplifier Antenna GPS Amplifier and GPS Repeater.
- [2] Florian Bousquet. 2017. Great solution for GPS sports watches.
- [3] Hugues Brenot, Witold Rohm, Michal Kačmarík, Gregor Möller, André Sá, Damian Tondaś, Lukas Rapant, Riccardo Biondi, Toby Manning, and Cédric Champollion. 2019. Cross-comparison and methodological improvement in GPS tomography. *Remote Sensing* 12, 1 (2019), 30.
- [4] Christina Chacour, Mehdi Naderi Soorki, Walid Saad, Mehdi Bennis, Petar Popovski, and Mérouane Debbah. 2022. Seven defining features of terahertz (THz) wireless systems: A fellowship of communication and sensing. *IEEE Communications Surveys & Tutorials* 24, 2 (2022), 967–993.
- [5] Kongyang Chen and Guang Tan. 2018. BikeGPS: Accurate localization of shared bikes in street canyons via low-level GPS cooperation. In *Proceedings of the 16th Annual International Conference on Mobile Systems, Applications, and Services*. 150–162.
- [6] Yunfei Chen, Jie Zhang, Wei Feng, and Mohamed-Slim Alouini. 2021. Radio sensing using 5G signals: Concepts, state of the art, and challenges. *IEEE Internet of Things Journal* 9, 2 (2021), 1037–1052.
- [7] Mostafa Zaman Chowdhury, Md Shahjalal, Shakil Ahmed, and Yeong Min Jang. 2020. 6G wireless communication systems: Applications, requirements, technologies, challenges, and research directions. *IEEE Open Journal of the Communications Society* 1 (2020), 957–975.
- [8] Minhao Cui, Binbin Xie, Qing Wang, and Jie Xiong. 2023. DancingAnt: Body-empowered Wireless Sensing Utilizing Pervasive Radiations from Powerline. In *Proceedings of ACM MobiCom*. 232–244.
- [9] Huixin Dong, Yirong Xie, Xianan Zhang, Wei Wang, Xinyu Zhang, and Jianhua He. 2023. GPSMirror: Expanding Accurate GPS Positioning to Shadowed and Indoor Regions with Backscatter. In *Proceedings of the 29th Annual International Conference on Mobile Computing and Networking*. 1–15.
- [10] Werner Enderle, Francesco Gini, Henno Boomkamp, Joel JK Parker, Benjamin W Ashman, Bryan W Welch, Mick Koch, and O Scott Sands. 2018. Space user visibility benefits of the multi-GNSS Space Service Volume: An internationally-coordinated, global and mission-specific analysis. In *Proceedings of the 31st international technical meeting of the satellite division of the institute of navigation (ION GNSS+ 2018)*. 1191–1207.
- [11] Yuda Feng, Yaxiong Xie, Deepak Ganeshan, and Jie Xiong. 2021. LTE-based pervasive sensing across indoor and outdoor. In *Proceedings of the 19th ACM Conference on Embedded Networked Sensor Systems*. 138–151.
- [12] Yuda Feng, Yaxiong Xie, Deepak Ganeshan, and Jie Xiong. 2022. Lte-based low-cost and low-power soil moisture sensing. In *Proceedings of the 20th ACM Conference on Embedded Networked Sensor Systems*. 421–434.
- [13] Ruiyang Gao, Mi Zhang, Jie Zhang, Yang Li, Enze Yi, Dan Wu, Leye Wang, and Daqing Zhang. 2021. Towards position-independent sensing for gesture recognition with Wi-Fi. *Proceedings of the ACM on Interactive, Mobile, Wearable and Ubiquitous Technologies* 5, 2 (2021), 1–28.
- [14] Google. 2016. GPS Measurement Tools. <https://github.com/google/gps-measurement-tools>.
- [15] Tianbo Gu, Zheng Fang, Zhicheng Yang, Pengfei Hu, and Prasant Mohapatra. 2019. Mmsense: Multi-person detection and identification via mmwave sensing. In *Proceedings of the 3rd ACM Workshop on Millimeter-wave Networks and Sensing Systems*. 45–50.
- [16] Philipp Hillger, Janusz Grzyb, Ritesh Jain, and Ullrich R Pfeiffer. 2018. Terahertz imaging and sensing applications with silicon-based technologies. *IEEE Transactions on Terahertz Science and Technology* 9, 1 (2018), 1–19.
- [17] Historytools.org. 2024. Starlink vs LTE: A Comprehensive Comparison for the Digital Divide.
- [18] Wenjun Jiang, Hongfei Xue, Chenglin Miao, Shiyang Wang, Sen Lin, Chong Tian, Srinivasan Murali, Haochen Hu, Zhi Sun, and Lu Su. 2020. Towards 3D human pose construction using wifi. In *26th Annual International Conference on Mobile Computing and Networking (MobiCom)*. ACM, 1–14.
- [19] Shuanggen Jin and Attila Komjathy. 2010. GNSS reflectometry and remote sensing: New objectives and results. *Advances in Space Research* 46, 2 (2010), 111–117.
- [20] Joseph B Keller. 1962. Geometrical theory of diffraction. *Josa* 52, 2 (1962), 116–130.
- [21] Derek Ka-Hei Lai, Li-Wen Zha, Tommy Yau-Nam Leung, Andy Yiu-Chau Tam, Bryan Pak-Hei So, Hyo-Jung Lim, Daphne Sze Ki Cheung, Duo Wai-Chi Wong, and James Chung-Wai Cheung. 2023. Dual ultra-wideband (UWB) radar-based sleep posture recognition system: Towards ubiquitous sleep monitoring. *Engineered Regeneration* 4, 1 (2023), 36–43.
- [22] Richard B Langley. 1997. GPS receiver system noise. *GPS world* 8, 6 (1997), 40–45.
- [23] Alfred Leick, Lev Rapoport, and Dmitry Tatarnikov. 2015. *GPS satellite surveying*. John Wiley & Sons.
- [24] Dong Li, Shirui Cao, Sungsoon Ivan Lee, and Jie Xiong. 2022. Experience: practical problems for acoustic sensing. In *Proceedings of the 28th Annual International Conference on Mobile Computing And Networking*. 381–390.
- [25] Xiang Li, Shengjie Li, Daqing Zhang, Jie Xiong, Yasha Wang, and Hong Mei. 2016. Dynamic-MUSIC: Accurate device-free indoor localization. In *Proceedings of the 2016 ACM international joint conference on pervasive and ubiquitous computing*. 196–207.
- [26] Haipeng Liu, Yuheng Wang, Anfu Zhou, Hanyue He, Wei Wang, Kunpeng Wang, Peilin Pan, Yixuan Lu, Liang Liu, and Huadong Ma. 2020. Real-time arm gesture recognition in smart home scenarios via millimeter wave sensing. *Proceedings of the ACM on interactive, mobile, wearable and ubiquitous technologies* 4, 4 (2020), 1–28.
- [27] Jian Liu, Hongbo Liu, Yingying Chen, Yan Wang, and Chen Wang. 2019. Wireless sensing for human activity: A survey. *IEEE Communications Surveys & Tutorials* 22, 3 (2019), 1629–1645.
- [28] Xiaochen Liu, Suman Nath, and Ramesh Govindan. 2018. Gnome: A practical approach to NLOS mitigation for GPS positioning in smartphones. In *Proceedings of the 16th Annual International Conference on Mobile Systems, Applications, and Services*. 163–177.
- [29] Shahriar Nirjon, Jie Liu, Gerald DeJean, Bodhi Priyantha, Yuzhe Jin, and Ted Hart. 2014. COIN-GPS: Indoor localization from direct GPS receiving. In *Proceedings of the 12th annual international conference on Mobile systems, applications, and services*. 301–314.
- [30] Kai Niu, Fusang Zhang, Jie Xiong, Xiang Li, Enze Yi, and Daqing Zhang. 2018. Boosting fine-grained activity sensing by embracing wireless multipath effects. In *ACM International Conference on emerging Networking EXperiments and Technologies (CONECT)*. ACM, 139–151.
- [31] Anurag Pallaprolu, Winston Hurst, Sophia Paul, and Yasamin Mostofi. 2023. I Beg to Diffract: RF Field Programming With Edges. In *Proceedings of the 29th Annual International Conference on Mobile Computing and Networking*. 1–15.
- [32] Anurag Pallaprolu, Belal Korany, and Yasamin Mostofi. 2022. Wiffract: a new foundation for RF imaging via edge tracing. In *Proceedings of the 28th Annual International Conference on Mobile Computing And Networking*. 255–267.
- [33] Debora Pastina, Fabrizio Santi, Federica Pieralice, Michail Antoniou, and Mikhail Cherniakov. 2020. Passive radar imaging of ship targets with GNSS signals of opportunity. *IEEE Transactions on Geoscience and Remote Sensing* 59, 3 (2020), 2627–2642.

- [34] João Pereira, Eugene Casmin, and Rodolfo Oliveira. 2023. A Passive RF Testbed for Human Posture Classification in FM Radio Bands. *Sensors* 23, 23 (2023), 9563.
- [35] Yili Ren, Zi Wang, Sheng Tan, Yingying Chen, and Jie Yang. 2021. Winect: 3d human pose tracking for free-form activity using commodity wifi. *ACM on Interactive, Mobile, Wearable and Ubiquitous Technologies (IMWUT)* 5, 4 (2021), 1–29.
- [36] Emad Hmood Salman, Nor Kamariah Noordin, Shaiful Jahari Hashim, Fazirulhisyam Hashim, and Chee Kyun Ng. 2017. An overview of spectrum sensing techniques for cognitive LTE and LTE-A radio systems. *Telecommunication Systems* 65 (2017), 215–228.
- [37] Shuyu Shi, Stephan Sigg, and Yusheng Ji. 2012. Passive detection of situations from ambient fm-radio signals. In *Proceedings of the 2012 ACM Conference on Ubiquitous Computing*. 1049–1053.
- [38] Raphael Stauffer, Roland Hohensinn, ID Herrera Pinzón, Gregor Moeller, Yuanxin Pan, Grzegorz Klopotek, Benedikt Soja, Elmar Brockmann, and Markus Rothacher. 2023. Estimation of tropospheric parameters with gnss smartphones in a differential approach. *Measurement Science and Technology* 34, 9 (2023), 095126.
- [39] U-blox. 2011. Meizu high-definition smartphone for China includes u-blox GPS.
- [40] U-blox. 2015. NEO-M8: U-blox M8 concurrent GNSS modules.
- [41] Fengyu Wang, Feng Zhang, Chenshu Wu, Beibei Wang, and KJ Ray Liu. 2020. Respiration tracking for people counting and recognition. *IEEE Internet of Things Journal* 7, 6 (2020), 5233–5245.
- [42] Hao Wang, Daqing Zhang, Junyi Ma, Yasha Wang, Yuxiang Wang, Dan Wu, Tao Gu, and Bing Xie. 2016. Human respiration detection with commodity WiFi devices: Do user location and body orientation matter?. In *Proceedings of the 2016 ACM international joint conference on pervasive and ubiquitous computing*. 25–36.
- [43] Tianlin Wang, Christopher S Ruf, Scott Gleason, Andrew J O'Brien, Darren S McKague, Bruce P Block, and Anthony Russel. 2021. Dynamic calibration of GPS effective isotropic radiated power for GNSS-reflectometry earth remote sensing. *IEEE Transactions on Geoscience and Remote Sensing* 60 (2021), 1–12.
- [44] Wei Wang, Alex X Liu, and Ke Sun. 2016. Device-free gesture tracking using acoustic signals. In *Proceedings of the 22nd Annual International Conference on Mobile Computing and Networking*. 82–94.
- [45] Xuanzhi Wang, Kai Niu, Jie Xiong, Bochong Qian, Zhiyun Yao, Tairong Lou, and Daqing Zhang. 2022. Placement matters: Understanding the effects of device placement for WiFi sensing. *Proceedings of the ACM on Interactive, Mobile, Wearable and Ubiquitous Technologies* 6, 1 (2022), 1–25.
- [46] Zhijun Wu, Rusan Liu, and Haijuan Cao. 2018. ECDSA-based message authentication scheme for BeiDou-II navigation satellite system. *IEEE Trans. Aerospace Electron. Systems* 55, 4 (2018), 1666–1682.
- [47] Binbin Xie, Minhao Cui, Deepak Ganesan, Xiangru Chen, and Jie Xiong. 2023. Boosting the Long Range Sensing Potential of LoRa. In *Proceedings of the 21st Annual International Conference on Mobile Systems, Applications and Services*. 177–190.
- [48] Binbin Xie, Deepak Ganesan, and Jie Xiong. 2022. Embracing lora sensing with device mobility. In *Proceedings of the 20th ACM Conference on Embedded Networked Sensor Systems*. 349–361.
- [49] Binbin Xie, Jie Xiong, Xiaojiang Chen, and Dingyi Fang. 2020. Exploring commodity rfid for contactless sub-millimeter vibration sensing. In *ACM Conference on Embedded Networked Sensor Systems (SenSys)*. 15–27.
- [50] Kun Yang, Xiaolong Zheng, Jie Xiong, Liang Liu, and Huadong Ma. 2022. WiImg: pushing the limit of WiFi sensing with low transmission rates. In *2022 19th Annual IEEE International Conference on Sensing, Communication, and Networking (SECON)*. IEEE, 1–9.
- [51] Youwei Zeng, Dan Wu, Jie Xiong, Jinyi Liu, Zhaopeng Liu, and Daqing Zhang. 2020. MultiSense: Enabling multi-person respiration sensing with commodity wifi. *Proceedings of the ACM on Interactive, Mobile, Wearable and Ubiquitous Technologies* 4, 3 (2020), 1–29.
- [52] Youwei Zeng, Dan Wu, Jie Xiong, Enze Yi, Ruiyang Gao, and Daqing Zhang. 2019. FarSense: Pushing the range limit of WiFi-based respiration sensing with CSI ratio of two antennas. *Proceedings of the ACM on Interactive, Mobile, Wearable and Ubiquitous Technologies* 3, 3 (2019), 1–26.
- [53] Daqing Zhang, Fusang Zhang, Dan Wu, Jie Xiong, and Kai Niu. 2021. Fresnel zone based theories for contactless sensing. *Contactless Human Activity Analysis* (2021), 145–164.
- [54] Fusang Zhang, Zhaoxin Chang, Jie Xiong, Junqi Ma, Jiazhi Ni, Wenbo Zhang, Beihong Jin, and Daqing Zhang. 2023. Embracing Consumer-level UWB-equipped Devices for Fine-grained Wireless Sensing. *ACM on Interactive, Mobile, Wearable and Ubiquitous Technologies (IMWUT)* 6, 4 (2023), 1–27.
- [55] Fusang Zhang, Zhi Wang, Beihong Jin, Jie Xiong, and Daqing Zhang. 2020. Your Smart Speaker Can "Hear" Your Heartbeat!. *Proceedings of the ACM on Interactive, Mobile, Wearable and Ubiquitous Technologies* 4, 4 (2020), 1–24.
- [56] Fusang Zhang, Jie Xiong, Zhaoxin Chang, Junqi Ma, and Daqing Zhang. 2022. Mobi2Sense: empowering wireless sensing with mobility. In *Proceedings of the 28th Annual International Conference on Mobile Computing And Networking*. 268–281.
- [57] Yanning Zhao, Toshiyuki Yamamoto, and Takayuki Morikawa. 2018. An analysis on older driver's driving behavior by GPS tracking data: Road selection, left/right turn, and driving speed. *Journal of traffic and transportation engineering (English edition)* 5, 1 (2018), 56–65.
- [58] Heng Zhou and Takuya Maekawa. 2023. GPS-assisted Indoor Pedestrian Dead Reckoning. *Proceedings of the ACM on Interactive, Mobile, Wearable and Ubiquitous Technologies* 6, 4 (2023), 1–36.
- [59] Juncen Zhu, Jannong Cao, Yanni Yang, Wei Ren, and Huizi Han. 2023. mmDrive: Fine-Grained Fatigue Driving Detection Using mmWave Radar. *ACM Transactions on Internet of Things* (2023).
- [60] Yongpan Zou, Jiang Xiao, Jinsong Han, Kaishun Wu, Yun Li, and Lionel M Ni. 2016. Grfid: A device-free rfid-based gesture recognition system. *IEEE Transactions on Mobile Computing* 16, 2 (2016), 381–393.